

Distinctive g -factor of moiré-confined excitons in van der Waals heterostructures

Y. Galvão Gobato,^{1,*} C. Serati de Brito,¹ A. Chaves,^{2,3,†} M. A. Prosnikov,⁴ T. Woźniak,⁵ Shi Guo,⁶ Ingrid D. Barcelos,⁷ M. V. Milošević,^{3,8} F. Withers,⁶ and P. C. M. Christianen⁴

¹*Physics Department, Federal University of São Carlos (UFSCAR)-Brazil*

²*Universidade Federal do Ceará, Departamento de Física, 60455-760 Fortaleza, Ceará, Brazil*

³*Department of Physics, University of Antwerp, Groenenborgerlaan 171, B-2020 Antwerp, Belgium*

⁴*High Field Magnet Laboratory (HFML-EMFL),*

Radboud University, 6525 ED, Nijmegen, The Netherlands

⁵*Department of Semiconductor Materials Engineering,*

Wrocław University of Science and Technology, 50-370 Wrocław, Poland

⁶*Centre for Graphene Science, College of Engineering,*

Mathematics and Physical Sciences, University of Exeter, Exeter, EX4 4QF

⁷*Brazilian Synchrotron Light Laboratory (LNLS),*

Brazilian Center for Research in Energy and Materials (CNPEM), 13083-970 Campinas, São Paulo, Brazil

⁸*NANOLab Center of Excellence, University of Antwerp, Belgium*

We investigated experimentally the valley Zeeman splitting of excitonic peaks in the photoluminescence (PL) spectra of high-quality hBN/WS₂/MoSe₂/hBN heterostructures at near-zero twist angles under perpendicular magnetic fields up to 20 T. We identify two neutral exciton peaks in the PL spectra: the lower energy one exhibits a reduced g -factor relative to that of the higher energy peak, and much lower than the recently reported values for interlayer excitons in other van der Waals (vdW) heterostructures. We provide evidence that such a discernible g -factor stems from the spatial confinement of the exciton in the potential landscape created by the moiré pattern, due to lattice mismatch and/or inter-layer twist in heterobilayers. This renders magneto- μ PL an important tool to reach deeper understanding of the effect of moiré patterns on excitonic confinement in vdW heterostructures.

Recent years have witnessed enormous interest in the optical properties of heterostructures based on monolayer transition-metal dichalcogenides (TMDs) [1, 2]. Monolayer TMDs exhibit a direct band gap at two inequivalent $\pm K$ valleys and enhanced excitonic effects due to strong out-of-plane quantum confinement, large in-plane carrier effective mass and significantly reduced Coulomb screening [3–6]. Large spin-orbit coupling and lack of inversion symmetry lift the spin degeneracy of the electron and hole states and therefore lock the spin and valley degrees of freedom [6–9]. As a consequence, the $\pm K$ valleys can be individually addressed using right- (σ_+) and left-handed (σ_-) circularly polarized light [10]. Under perpendicular external magnetic fields, valley Zeeman effects and magnetic-field-induced valley polarization can be observed [11–18].

TMD heterostructures with stacking angles near either 0° (AA stacking) or 60° (AB stacking) exhibit pronounced emission from both inter-layer and intra-layer excitons [19–22]. They both present large exciton binding energies (>100 meV) and are highly robust against dissociation under applied electric fields, which opens up new opportunities to investigate valley–spin optoelectronics [23, 24]. The lattice mismatch between the materials that compose the heterostructure, combined with small inter-layer twist angles, lead to a moiré pattern consisting of regions where the crystal exhibits stacking registries that are locally different along the materials plane [25]. Recent experiments have shown evidence that such different local crystal properties in the moiré pattern effectively

produce a potential landscape strong enough to localize both inter- and intra-layer exciton wave functions and thus produce quantized exciton states [26], which brings the possibility of using moiré-confined excitons as single-photon emitters and quantum simulators [27, 28].

It was previously shown that the effective g -factor of inter-layer excitons (iXs) depends on the twist angle between the layers of van der Waals heterostructures (vdWHSs) [29]. Several experimental studies of MoSe₂/WSe₂ heterostructures have shown an effective g -factor of iXs of $g \approx +6$ for twist angles near 0° , while $g \approx -15$ was found for twist angles around 60° [21, 29, 30]. These values are very different from reported g -factors of intra-layer excitons in individual monolayer TMDs ($g \approx -4$) [12, 14, 15, 29]. In fact, the value of effective exciton g -factor results from spin and orbital angular momenta of electron and hole bands, while its sign is governed by optical selection rules [31, 32]. As a consequence, it is significantly affected by the materials composition, inter-layer exciton hybridization, and even by the spread of the exciton wave function [33]. In the presence of the effective confining potential produced by the moiré pattern, the confined exciton wave function in reciprocal space is expected to populate regions away from the K-point edge of the Brillouin zone, thus effectively modifying the exciton g -factor, which can in turn be used to probe the moiré exciton confinement.

In this work we experimentally analyze the exciton g -factors in a MoSe₂/WS₂ heterobilayer with near-zero twisting angle. Due to the relatively large lattice mis-

match between these two TMDs, strong moiré exciton confinement is expected, even for a negligible inter-layer twist as in our samples. Our magneto-photoluminescence (magneto- μ PL) data reveal the existence of two neutral exciton peaks, at different energies. The effective g -factor of the lower-energy exciton is consistently lower as compared to either the perfectly charge-separated inter-layer excitons observed in MoSe₂/WSe₂ (and other) heterobilayers, or the intra-layer excitons either in an individual MoSe₂ monolayer or in MoSe₂/WS₂ heterobilayers. We argue that the low energy PL peak is due to an exciton whose center-of-mass motion is confined by the moiré potential landscape, as evidenced by the peak identified as the MoSe₂ intra-layer exciton (with an experimentally validated g -factor).

The monolayers of MoSe₂ and WS₂ were obtained by mechanical exfoliation from bulk single crystals from HQ Graphene. The heterostructures were fabricated by an all-dry transfer technique and consist of a monolayer of MoSe₂ on a monolayer of WS₂, sandwiched between two thin sheets of hexagonal boron nitride (hBN). The small stacking angle $\approx 0^\circ$ is obtained by controlling the orientation of the edges of the cleaved flakes and the crystal direction. For μ PL measurements, the sample was placed on a x - y - z piezoelectric Attocube stage and cooled down to 4.2 K in a cryostat placed inside a 30 T resistive magnet. The μ PL measurements were performed using a continuous-wave Millennia Spectra Physics laser excitation with a photon energy of 2.33 eV. The laser was focused on the flake by an $40\times$ Attocube objective (NA = 0.55) with a spot size of about $4\ \mu\text{m}$. The μ PL signal was collected with appropriate optics in backscattering configuration and measured by a Princeton Instruments Acton spectrometer connected with a liquid-nitrogen cooled charge-coupled device. The polarization-resolved excitation and μ PL collection were performed using quarter-wave plates and linear polarizers. The sample was mounted with its normal parallel to the magnetic field direction (Faraday configuration) and kept at a temperature of 4.2 K. We have measured the μ PL at several laser positions on the heterostructure region, which allowed us to verify the consistency of our findings. All results reported in this Letter are taken at a single location in the sample, while results for other locations are made available in the Supplemental Material (SM) [34].

As shown in Fig. 1(a), the PL spectrum of the MoSe₂/WS₂ vdWHS, whose optical microscopy image is shown in the inset, measured in absence of an applied magnetic field, exhibits two peaks associated to the neutral excitons, labeled mX (1.603 eV) and X_A (1.646 eV), interspersed by trion peaks mX* (1.570 eV) and X* (1.619 eV). These results are very similar to previous experimental results reported for MoSe₂/WS₂ heterobilayers [35, 36]. We note the energy separation between the mX and X_A PL peak positions of ≈ 43 meV. The energy separation between X_A and X* is 27 meV, whereas

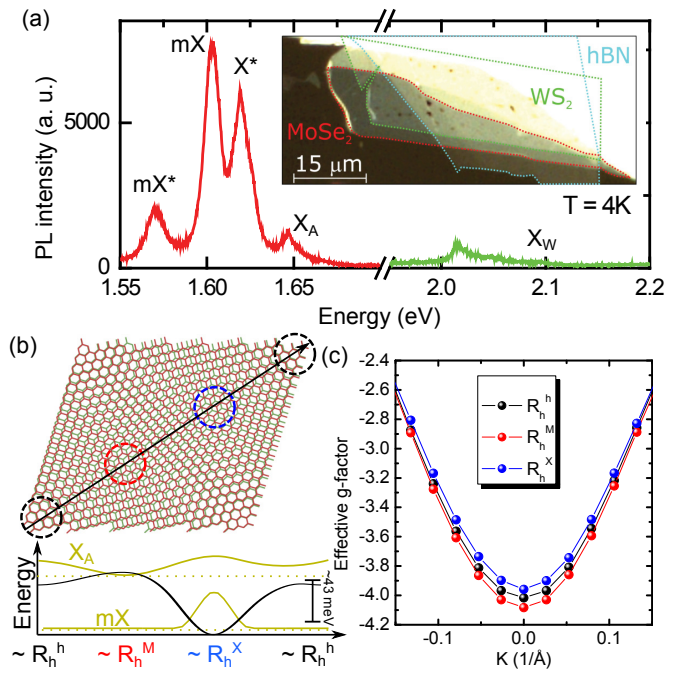


FIG. 1. (Color online) (a) Typical PL spectrum of the MoSe₂/WS₂ vdWHS at 4 K. The inset shows the optical image of the sample. The intersection of red (MoSe₂) and green (WS₂) delimited areas highlights the vdWHS region. PL of the monolayer WS₂ region of the sample (green data points) shows features at higher energies, identified as the monolayer exciton X_W peak for this material, whereas the lower energy features are identified as the free (moiré-confined) MoSe₂ intra-layer exciton X_A (mX) and trion X* (mX*). (b) Sketch of the crystal structure of a MoSe₂/WS₂ vdWHS with a twist angle ≈ 0 . Local stacking registries R_h^h , R_h^M and R_h^X , highlighted respectively by black, red, and blue circles, form a periodic moiré pattern. The quasi-particle energy gap is locally different in each of these regions, thus producing a moiré potential landscape for excitons. This is illustrated by the black line in the bottom panel, which depicts the quasi-particle gap along the arrow drawn in the top panel. The mX and X_A peaks in the PL spectrum originate respectively from confined and (nearly) free excitons in the moiré pattern, whose wave functions are represented by yellow curves in the bottom panel. (c) Effective g -factor dispersion for the intra-layer MoSe₂ exciton in the vicinity of the K-point, as obtained by DFT calculations assuming the three stacking registries identified in (b).

between mX* and mX peaks a splitting of 33 meV was observed. The energy separations are consistent with the identification of mX* and X* as trion emissions. Our laser power dependence study of all observed PL bands at 4 K (Fig. S3 in the SM [34]) provides further support to this interpretation of the excitonic nature of different PL peaks. We thus correlate the experimentally observed mX peak to a moiré-confined exciton state, whereas the X_A peak is interpreted as the emission from an unconfined intra-layer MoSe₂ exciton [35–37], as will be detailed further below.

In order to understand the origin of the two neutral exciton peaks consistently observed in our experiments, let us consider a van der Waals stacked MoSe₂/WS₂ heterobilayer with inter-layer twist angle $\approx 0^\circ$, as sketched in Fig. 1(b). The periodic moiré pattern created by the lattice mismatch between the layers exhibits regions with local stacking registries identified as R_h^h , R_h^M and R_h^X , marked as black, red, and blue circles, respectively. Since the quasi-particle gap of each of these registries is different, one expects these regions to form a periodic landscape of potential wells and barriers for the exciton [26], as illustrated by the black line in the bottom panel of Fig. 1(b). The quasi-particle gaps obtained from ab initio calculations with hybrid functional (HSE06) in a MoSe₂/WS₂ vdWHS with R_h^h , R_h^M and R_h^X are 1.830 eV, 1.831, and 1.816 eV, respectively. All three cases exhibit practically the same effective mass and, consequently, the same binding energy 0.230 eV, thus explaining the experimentally observed peaks around 1.6 eV. In the R_h^X case, however, the theoretically predicted exciton energy is at least 15 meV lower than those of R_h^h and R_h^M , thus working as a confining well for the exciton center-of-mass. Since the inter-atomic distances in the actual vdWHS crystal are likely different from those in our simulations for pure R_h^h , R_h^M and R_h^X crystals, which were artificially strained to produce commensurate lattices, and our calculations for local quasi-particle gaps were made without GW corrections, the actual moiré confinement potential in the MoSe₂/WS₂ vdWHS is likely to be significantly stronger than the ≈ 15 meV predicted here.

The valence band edges of the isolated monolayers are separated by ≈ 750 meV [38], which restricts the holes in the lowest energy exciton states to the MoSe₂ layer. Conversely, the conduction band offset between the individual monolayers is small: for instance, Refs. [35] and [36] suggest conduction band offsets of 13 meV and 5.8 meV, respectively, with lowest energy electrons also in the MoSe₂ layer. Ab initio calculations in Ref. [38] give somewhat higher values for this band offset, but all results in the literature point towards a type-I band alignment for this combination of materials.[39] Therefore, in principle, the lowest energy exciton state in this vdWHS must have a dominant intra-layer MoSe₂ component, although, due to such low conduction band offset, hybrid states with an inter-layer component, where electrons partially populate the WS₂ layer as well, may also be possible.

The interplay between the effects of the moiré confinement potential and inter-layer hybridization in MoSe₂/WS₂ heterostructures has been thoroughly investigated in Ref. [35], where PL spectra were observed with the same four peaks reported here, considering a similar interpretation for X_A and mX, but emphasizing a possibility of inter-layer hybridization in the latter. On the other hand, the exciton Stark shift measurements reported in Ref. [37] provided strong evidence that the \approx

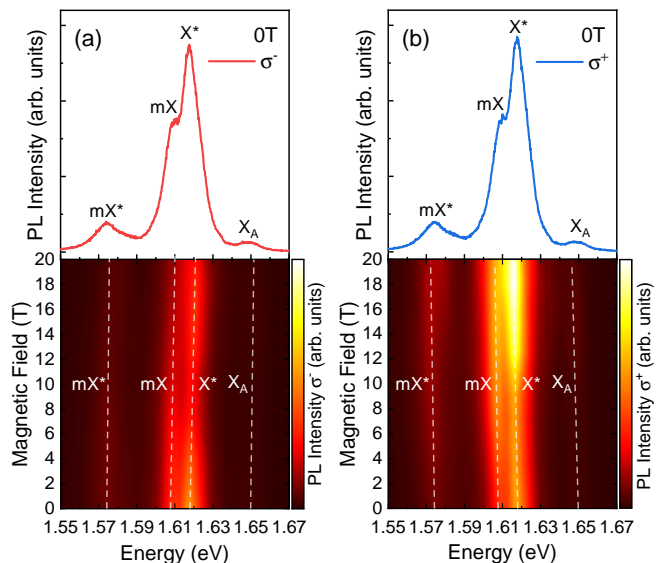


FIG. 2. (Color online) Typical spectra at 0 T (top panels) for the MoSe₂/WS₂ vdWHS at 4 K and the corresponding color-code map of the PL intensity versus energy and magnetic field (bottom panels), for (a) σ_- and (b) σ_+ light polarizations.

1.60 eV signal (mX) in this system does not exhibit a significant out-of-plane dipole moment (i.e., high contribution from an inter-layer component), but rather stems from a virtually pure intra-layer exciton, fully consistent with the type-I band alignment. With that in mind, we will neglect the inter-layer contribution to the mX peak and focus primarily on the in-plane moiré confinement of the intra-layer exciton and how it affects the effective exciton g -factor for this peak under applied magnetic field.

In the presence of a perpendicularly applied magnetic field $\vec{B} = B\hat{z}$, the energy of each exciton state shifts as

$$E_i(B) = E_i(0) \pm g_i \mu_B B / 2, \quad (1)$$

where μ_B is the Bohr magneton, B the magnetic field strength, $i = \text{mX}, \text{mX}^*, \text{X}^*$ or X_A , the \pm sign depends on the valley degree of freedom, associated with the circular polarization σ_{\pm} , and the linear term corresponds to the Zeeman shift, with an effective Landé g -factor g_i . The quadratic (diamagnetic) shifts for each exciton state are an order of magnitude lower than the Zeeman shifts and are therefore neglected. These g -factors are directly related to the angular momenta of the valence and conduction band states involved in the exciton transition. Although a survey of such angular momenta values for several monolayer TMDs, along with a thorough description of the calculation method, can be found in Ref. [31], we briefly describe the theoretical procedure to obtain effective exciton g -factors from density functional theory calculations in the SM [34], for the sake of completeness.

Results in Fig. 1(c) demonstrate that the angular momenta of the conduction and valence band states in a

MoSe₂/WS₂ vdWHS with three different stacking registries observed for $\approx 0^\circ$ twist angle in Fig. 1(b) are not significantly different from that of the isolated MoSe₂ monolayer, which is $g \approx -4$ [31]. On the other hand, they are strongly reduced in modulus for exciton momenta away from the exciton band edge, ranging from $-4.1 < g < -3.9$ exactly at the K point, down to $g \approx -2.6$ for momenta 0.15 \AA^{-1} away from this point. This demonstrates that if the exciton center-of-mass momentum is effectively non-zero, the exciton g -factor is expected to be reduced. In fact, the momentum of a ground-state exciton that is quantum confined by an external potential is naturally non-zero. The moiré potential illustrated in the bottom panel of Fig. 1(b), with minima at the R_h^X regions, suggests that the exciton center-of-mass is effectively quantum confined to these regions, which allows one to predict a significant reduction in the g -factors for moiré confined exciton states. Wave functions of shallow (X_A) and (mX) confined exciton states are depicted by yellow lines in the bottom panel of Fig. 1(b).

Figure 2 shows the magnetic field dependence of the PL spectrum for the left (σ_- , a) and right (σ_+ , b) circularly polarized emissions in a magnetic field up to 20 T for another laser position as compared to Figure 1. With increasing magnetic field, we observe that all PL peak energies shift monotonically. A red/blue shift of the circularly polarized σ_+/σ_- PL peak positions was observed with increasing magnetic field, which clearly evidences the regular valley Zeeman splitting effect [11–18]. The perpendicular magnetic field removes the valley degeneracy and splits the PL peaks with Zeeman energies that depend linearly on the field. Furthermore, the $\sigma_+(\sigma_-)$ polarized PL intensities increase (decrease) significantly with field evidenced by the brighter(darker) colors in Fig. 2(b). Similar behavior was observed for μ PL data obtained at different laser positions of the heterostructure (see Figs. S4 and S5 in the SM [34]).

We have determined the peak energies of the mX, mX*, X_A and X^* emission lines as a function of magnetic field by fitting each PL peak with a Voigt line shape. The resulting field dependence of peak energies is plotted in Fig. 3(a). Measurements at all the positions across the heterostructure exhibit a valley splitting that clearly follows a linear dependence with magnetic field. The effective g -factors for all emission peaks are obtained by fitting the experimental Zeeman shifts to $\Delta E_i = E_i^{\sigma_+} - E_i^{\sigma_-} = g_i \mu_B B$ (Fig. 3(b-e)). This yields g -factors ≈ -4.4 for both the X_A and X^* PL peaks. Lower g -factors are observed for the mX* trion and mX exciton, with values $g_{mX^*} = -3.3$ and $g_{mX} = -3.5$, respectively. These values are also lower than the effective g -factors of excitons in monolayer MoSe₂, with $g_A \approx -4$ in previous works [40]. In fact, we consistently observe reduced effective g -factors for the mX and mX* PL peaks for all measured laser positions within the heterostructure re-

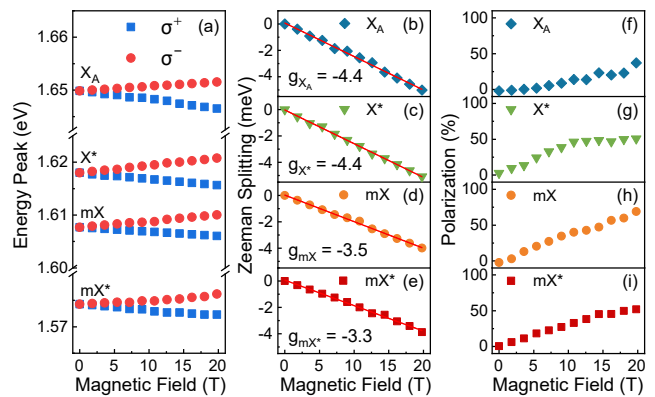


FIG. 3. (Color online) Effective g -factors of the exciton peaks in hBN encapsulated MoSe₂/WS₂ vdWHS. (a) Magnetic field dependence of the PL peak energies for σ_+ and σ_- polarization. (b)-(e) Zeeman splitting of each PL peak as a function of magnetic field. Solid lines are linear fits to the data. (f)-(i) Circular polarization degree as a function of the magnetic field.

gion.

As previously discussed, moiré confined excitons are expected to exhibit reduced g -factors. We therefore address the X_A peak as either free or shallow-confined exciton states in the higher energy R_h^h and R_h^M regions, whereas mX is interpreted as a moiré-confined exciton state at the R_h^X region, with lower energy and, consequently, non-zero center-of-mass momentum. This interpretation of X_A and mX matches the findings of earlier works [35], except for our assumption of weak inter-layer hybridization in mX, in accordance with Ref. [37]. The observed g -factor reduction evidences the effect of moiré confinement on the exciton effective angular momentum, which is the main finding of this work.

Let us compare the experimentally observed $\approx 22\%$ difference between g_A and g_{mX} with the theoretical predictions in Fig. 1(c). The predicted g -factor for nearly free intra-layer MoSe₂ excitons is $g_A \approx -4$. A 22% lower value for the moiré exciton yields $g_{mX} \approx -3.12$ which, according to Fig. 1(c), requires an exciton momentum $K \approx 0.11 \text{ \AA}^{-1}$. This corresponds to a confined state with energy roughly $\hbar^2 K^2 / 2M \approx 40 \text{ meV}$ below that of the free exciton, where we used the exciton effective mass $M = 1.094m_0$, as obtained from DFT. Indeed, this is in excellent agreement with the experimentally observed 43 meV separation between X_A and mX exciton peaks in the PL spectra. Moreover, this energy is also in the same order of magnitude as the one observed for similar moiré-confined excitons in Ref. [26].

The degree of valley polarization, defined as $P = (I^{\sigma_+} - I^{\sigma_-}) / (I^{\sigma_+} + I^{\sigma_-})$, is shown in Fig. 3(f-i) as a function of the field for each excitonic peak under circular polarization excitation. While P is zero for all peaks in the absence of an applied magnetic field, the mX excitons

exhibit a circular polarization as large as $\approx 70\%$ at field of 20 T, a nearly twice stronger polarization compared to the free X_A exciton at this field. This corroborates the interpretation of X_A as a predominantly intra-layer, nearly free, exciton, whose fast decay and relatively short lifetime limit the value of the field-induced valley polarization. On the other hand, the trion (X^*) has higher polarization degree, as it usually presents higher PL decay time and much longer intervalley scattering time [41]. As the polarization degree depends on the ratio of the PL decay and intervalley scattering times, the high polarization degree for mX suggests an important increase of intervalley scattering times for the moiré confined exciton, as compared to that for X_A . However, further studies would be necessary to understand in more detail the observed magnetic field dependence of the polarization degree of the moiré confined exciton.

Notice that, despite the qualitative agreement between the g -factors of the different mX and X_A peaks observed in our μ PL experiment and their theoretically predicted values, the latter are quantitatively lower. In fact, g -factors of X_A in MoSe₂ and WS₂ monolayers obtained by ab initio calculations are already slightly underestimated as compared to existing experimental data in the literature [31]. Nevertheless, our model shows that the distinctly lower g -factors for mX states, consistently observed in the experiments, are a direct consequence of the fact that the exciton wave function is quantum confined by the moiré pattern.

Assuming a possible inter-layer hybridization for mX [35], where electrons are shared between both layers due to the low conduction band offset of this vdWHS, our DFT calculations predict an even lower exciton g -factor, as a consequence of the lower angular momentum for conduction band electrons in the WS₂ layer [34]. This indicates that the g -factor of these excitons could be further controlled e.g. by an external electric field, perpendicular to the vdWHS plane, which would push electrons and holes towards different layers. The fact that the exciton g -factors observed here in MoSe₂/WS₂ vdWHS are similar or even reduced as compared to those of excitons in monolayer MoSe₂, is also in stark contrast to the g -factors of excitons in other similar heterostructures, such as MoSe₂/WSe₂ vdWHS [29], where exciton g -factors in the vdWHS are rather *enhanced* as compared to those of either monolayer MoSe₂ or WSe₂.

For twist angles around 60°, the inter-layer exciton g -factors are expected to be higher due to the sign change of the angular momentum for the conduction band states for these excitons [31]. Indeed, significantly higher values for iX g -factors in MoSe₂/WSe₂ vdWHS with 60° twist angle are observed in Ref. 29 for this reason. However, since the mX and X_A states in MoSe₂/WS₂ vdWHS have a strong intra-layer component and low inter-layer contribution [37], our model estimates the g -factors in $\theta \approx 60^\circ$ twisted MoSe₂/WS₂ heterostructures to be sim-

ilar to those for $\theta \approx 0^\circ$, in contrast to MoSe₂/WSe₂ vdWHS. Indeed, we experimentally verified this prediction with a 60° MoSe₂/WSe₂ vdWHS sample, for which the experimental results are detailed and discussed in the supplemental material.

In conclusion, we have measured the polarization-resolved photoluminescence of exciton states in high quality hBN-encapsulated MoSe₂/WS₂ heterostructures with near-zero stacking angle, under perpendicular magnetic fields up to 20 T. Two PL peaks are identified as due to exciton states predominantly with an intra-layer MoSe₂ component: one originates from a free exciton state, with higher energy, whereas the lower energy peak is identified as the moiré-confined exciton. The energy separation between these peaks suggests a moiré confinement energy of 43 meV, with respect to the free exciton state, which matches theoretical estimates. Both exciton energies shift linearly with magnetic field, but the moiré-confined exciton exhibits reduced g -factors compared to the unconfined one. This is a consequence of the quantized center-of-mass momentum of the moiré-confined exciton, which makes it probe regions of the Brillouin zone where the angular momentum state of the electron-hole pair is significantly reduced, as demonstrated by our calculations. By generalization of this finding we envision different possible behavior of exciton g -factors at different stacking angles, or in vdWHS composed of other combinations of 2D TMDs, where exciton confinement can be further enhanced e.g. by application of an interlayer electrostatic bias [42]. As a common denominator, we postulate that moiré-confined excitons in vdW heterostructures are discernible through their g -factors, which offers a fresh perspective on further studies of moiré excitons, especially in twisted bilayers, or under controlled strain and gating, where further rich manifestations of exciton physics are expected.

Acknowledgements This work was supported by HFML-RU/NWO-I, member of the European Magnetic Field Laboratory (EMFL). This work was also financially supported by the Brazilian Council for Research (CNPq), through the PRONEX/FUNCAP, Universal, and PQ programs (311678/2020-3), and the Research Foundation - Flanders. CSB acknowledges the financial support from CAPES fellowship and YGG acknowledges the financial support from FAPESP (grants 2018/01808-5, 2019/14017-9 and 2019/23488-5) and CNPQ (grants 311678/2020-3 and 426634/2018-7). TW acknowledges financial support from National Science Centre, Poland under grant 2021/41/N/ST3/04516. DFT calculations were performed with the support of the Interdisciplinary Centre for Mathematical and Computational Modelling (ICM) University of Warsaw and Center for Information Services and High Performance Computing (ZIH) at TU Dresden.

- * yara@df.ufscar.br
† andrej@fisica.ufc.br
- [1] A. K. Geim and I. V. Grigorieva, *Nature* **499**, 419 (2013).
 - [2] K. Novoselov, A. Mishchenko, A. Carvalho, and A. C. Neto, *Science* **353** (2016).
 - [3] K. F. Mak, C. Lee, J. Hone, J. Shan, and T. F. Heinz, *Physical Review Letters* **105**, 2 (2010).
 - [4] A. Splendiani, L. Sun, Y. Zhang, T. Li, J. Kim, C. Y. Chim, G. Galli, and F. Wang, *Nano Letters* **10**, 1271 (2010).
 - [5] X. Xu, W. Yao, D. Xiao, and T. F. Heinz, *Nature Physics* **10**, 343 (2014).
 - [6] D. Xiao, G. B. Liu, W. Feng, X. Xu, and W. Yao, *Physical Review Letters* **108**, 1 (2012).
 - [7] K. F. Mak, K. He, J. Shan, and T. F. Heinz, *Nature Nanotechnology* **7**, 494 (2012).
 - [8] H. Zeng, J. Dai, W. Yao, D. Xiao, and X. Cui, *Nature Nanotechnology* **7**, 490 (2012).
 - [9] J. R. Schaibley, H. Yu, G. Clark, P. Rivera, J. S. Ross, K. L. Seyler, W. Yao, and X. Xu, *Nature Reviews Materials* **1**, 1 (2016).
 - [10] S. Ishii, N. Yokoshi, and H. Ishihara, in *Journal of Physics: Conference Series*, Vol. 1220 (IOP Publishing, 2019) p. 012056.
 - [11] G. Aivazian, Z. Gong, A. M. Jones, R. L. Chu, J. Yan, D. G. Mandrus, C. Zhang, D. Cobden, W. Yao, and X. Xu, *Nature Physics* **11**, 148 (2015).
 - [12] Y. Li, J. Ludwig, T. Low, A. Chernikov, X. Cui, G. Arefe, Y. D. Kim, A. M. V. D. Zande, A. Rigosi, H. M. Hill, S. H. Kim, J. Hone, Z. Li, D. Smirnov, and T. F. Heinz, *Physical Review Letters* **113**, 1 (2014).
 - [13] A. Srivastava, M. Sidler, A. V. Allain, D. S. Lembke, A. Kis, and A. Imamoglu, *Nature Physics* **11**, 141 (2015).
 - [14] D. Macneill, C. Heikes, K. F. Mak, Z. Anderson, A. Kormányos, V. Zolyomi, J. Park, and D. C. Ralph, *Physical Review Letters* **114**, 1 (2015).
 - [15] G. Wang, L. Bouet, M. M. Glazov, T. Amand, E. L. Ivchenko, E. Palleau, X. Marie, and B. Urbaszek, *2D Materials* **2**, 34002 (2015).
 - [16] A. A. Mitioglu, P. Plochocka, G. D. Aguila, P. C. Christianen, G. Deligeorgis, S. Anghel, L. Kulyuk, and D. K. Maude, *Nano Letters* **15**, 4387 (2015).
 - [17] A. V. Stier, K. M. McCreary, B. T. Jonker, J. Kono, and S. A. Crooker, *Nature Communications* **7**, 1 (2016).
 - [18] G. Plechinger, P. Nagler, A. Arora, A. G. D. Águila, M. V. Ballottin, T. Frank, P. Steinleitner, M. Gmitra, J. Fabian, P. C. Christianen, R. Bratschitsch, C. Schüller, and T. Korn, *Nano Letters* **16**, 7899 (2016).
 - [19] P. Rivera, K. L. Seyler, H. Yu, J. R. Schaibley, J. Yan, D. G. Mandrus, W. Yao, and X. Xu, *Science* **351**, 688 (2016).
 - [20] P. K. Nayak, Y. Horbatenko, S. Ahn, G. Kim, J. U. Lee, K. Y. Ma, A. R. Jang, H. Lim, D. Kim, S. Ryu, H. Cheong, N. Park, and H. S. Shin, *ACS Nano* **11**, 4041 (2017).
 - [21] P. Nagler, M. V. Ballottin, A. A. Mitioglu, F. Mooshammer, N. Paradiso, C. Strunk, R. Huber, A. Chernikov, P. C. Christianen, C. Schüller, and T. Korn, *Nature Communications* **8**, 1 (2017).
 - [22] M. Förg, A. S. Baimuratov, S. Y. Kruchinin, I. A. Vovk, J. Scherzer, J. Förste, V. Funk, K. Watanabe, T. Taniguchi, and A. Högele, *Nature Communications* **12**, 1 (2021).
 - [23] P. Rivera, H. Yu, K. L. Seyler, N. P. Wilson, W. Yao, and X. Xu, *Nature Nanotechnology* **13**, 1004 (2018).
 - [24] A. Tartakovskii, *Nature Reviews Physics* **2**, 8 (2020).
 - [25] M. Kuwabara, D. R. Clarke, and D. Smith, *Applied physics letters* **56**, 2396 (1990).
 - [26] K. Tran, G. Moody, F. Wu, X. Lu, J. Choi, K. Kim, A. Rai, D. A. Sanchez, J. Quan, A. Singh, *et al.*, *Nature* **567**, 71 (2019).
 - [27] H. Baek, M. Brotons-Gisbert, Z. Koong, A. Campbell, M. Rambach, K. Watanabe, T. Taniguchi, and B. D. Gerardot, *Science advances* **6**, eaba8526 (2020).
 - [28] D. Huang, J. Choi, C.-K. Shih, and X. Li, *Nature Nanotechnology* , 1 (2022).
 - [29] K. L. Seyler, P. Rivera, H. Yu, N. P. Wilson, E. L. Ray, D. G. Mandrus, J. Yan, W. Yao, and X. Xu, *Nature* **567**, 66 (2019).
 - [30] M. Förg, A. S. Baimuratov, S. Y. Kruchinin, I. A. Vovk, J. Scherzer, J. Förste, V. Funk, K. Watanabe, T. Taniguchi, and A. Högele, *Nature communications* **12**, 1 (2021).
 - [31] T. Woźniak, P. E. F. Junior, G. Seifert, A. Chaves, and J. Kunstmann, *Physical Review B* **101**, 235408 (2020).
 - [32] T. Deilmann, P. Krüger, and M. Rohlfing, *Physical review letters* **124**, 226402 (2020).
 - [33] S.-Y. Chen, Z. Lu, T. Goldstein, J. Tong, A. Chaves, J. Kunstmann, L. Cavalcante, T. Wozniak, G. Seifert, D. Reichman, *et al.*, *Nano letters* **19**, 2464 (2019).
 - [34] See Supplemental Material for additional measurements at different positions in the sample.
 - [35] E. M. Alexeev, D. A. Ruiz-Tijerina, M. Danovich, M. J. Hamer, D. J. Terry, P. K. Nayak, S. Ahn, S. Pak, J. Lee, J. I. Sohn, *et al.*, *Nature* **567**, 81 (2019).
 - [36] L. Zhang, Z. Zhang, F. Wu, D. Wang, R. Gogna, S. Hou, K. Watanabe, T. Taniguchi, K. Kulkarni, T. Kuo, *et al.*, *Nature communications* **11**, 5888 (2020).
 - [37] Y. Tang, J. Gu, S. Liu, K. Watanabe, T. Taniguchi, J. Hone, K. F. Mak, and J. Shan, *Nature Nanotechnology* **16**, 52 (2021).
 - [38] S. Haastруп, M. Strange, M. Pandey, T. Deilmann, P. S. Schmidt, N. F. Hinsche, M. N. Gjerding, D. Torelli, P. M. Larsen, A. C. Riis-Jensen, *et al.*, *2D Materials* **5**, 042002 (2018).
 - [39] Y. Tang, J. Gu, S. Liu, K. Watanabe, T. Taniguchi, J. C. Hone, K. F. Mak, and J. Shan, arXiv preprint arXiv:2201.12510 (2022).
 - [40] M. Koperski, M. R. Molas, A. Arora, K. Nogajewski, M. Bartos, J. Wyzula, D. Vaclavkova, P. Kossacki, and M. Potemski, *2D Materials* **6**, 10.1088/2053-1583/aae14b (2019).
 - [41] Y. Zhang, K. Shinokita, K. Watanabe, T. Taniguchi, Y. Miyauchi, and K. Matsuda, *Advanced Functional Materials* **31**, 2006064 (2021).
 - [42] H. Yu, G.-B. Liu, J. Tang, X. Xu, and W. Yao, *Science advances* **3**, e1701696 (2017).